IUST Iran University of Science and Technology

Iranian Journal of Electrical and Electronic Engineering

Journal Homepage: ijeee.iust.ac.ir

Advanced GLONASS Satellite Simulator Based on Fuzzy Logic for Optimizing Navigation Precision through Enhanced GDOP

N. Dabaghi Daryan*, M. R. Mosavi*(C.A.), S. Mirzakuchaki*, and S. Tohidi*

Abstract: GNSS simulators are essential tools for testing and validating satellite navigation system receivers across various civil applications. This study introduces an improved GLONASS satellite simulator to optimize navigation precision by enhancing the satellite constellation's Dilution of Precision (DOP). The proposed simulator operates in two steps. In the first step, the system performs a full-day search to identify time intervals with minimal DOP using a local moving-average technique. In the second step, the impact of adding one virtual satellite—selected using fuzzy logic and evaluated through the Residual Geometric Dilution of Precision (RGDOP) metric—is examined to minimize Geometric Dilution of Precision (GDOP). The fuzzy system uses two inputs (RGDOP and elevation angle), where RGDOP is modeled with four Gaussian membership functions (very small, small, medium, large), and the elevation angle is modeled with three triangular membership functions (small, medium, large). These scenarios are tested on a Software-Defined Radio (SDR) and then a u-blox M8 receiver to evaluate and compare improvements in positioning accuracy across the tuned configurations. The results show that both optimization stages lead to significant gains in navigation performance. The first scenario leads to a 24.4% improvement in accuracy, while the second scenario achieves an even greater enhancement of 54.9%, highlighting the effectiveness of these approaches in reducing positioning error.

Keywords: GLONASS, Signal Modeling, Elevation, GDOP Optimization, Satellite Constellation Design, Fuzzy Weighted Logic, GNSS Simulation.

1 Introduction

Global Navigation Satellite Systems (GNSS) have attracted considerable interest due to the increasing reliance on GNSS-based navigation in both civilian and military applications [1]. GNSS, such as GLONASS, provide critical Positioning, Navigation, and Timing (PNT) services that enable accurate geolocation information globally. This technology is extensively used in fields such as surveying, mapping, robotics, healthcare, autonomous vehicles, marine, and aviation industries under diverse conditions where precise location and timing are crucial [2]. In mapping and surveying, GNSS enables detailed geographic data essential for urban planning, land management, and environmental monitoring. Autonomous and semi-autonomous vehicles depend on satellite positioning for safe navigation, efficient routing, and real-time decision-making. In robotics, GNSS is essential for guiding machines through hazardous environments where human intervention is

Iranian Journal of Electrical & Electronic Engineering, YYYY.
Paper first received DD MONTH YYYY and accepted DD MONTH YYYY.
* The authors are with the School of Electrical Engineering, Iran University of Science and Technology (IUST), Narmak, Tehran 16846-13114, Iran.

E-mails: n_dabaghi96@elec.iust.ac.ir, m_mosavi@iust.ac.ir, m_kuchaki@iust.ac.ir, and s_tohidi@elec.iust.ac.ir.
Corresponding Author: M. R. Mosavi

In Press

unsafe, supporting operations in areas like mining, and nuclear facilities. Additionally, healthcare applications are emerging, with GNSS supporting mobile medical devices and telemedicine, where accurate location data can improve patient outcomes, particularly in remote areas. Moreover, GNSS is necessary for telecommunications and timing systems, validating synchronization protocols critical for cellular networks, financial transactions, and power grids. As demand for precise navigation continues to grow, innovations focused on enhancing the accuracy and reliability of GNSS, including GLONASS, are becoming increasingly vital [3]. GNSS observations suffer from several errors, including satellite-related ephemeris errors (orbit error, clock error, and signal bias), transmission-related atmosphere delay (ionospheric and tropospheric), and receiver-related observation error, which degrades the positioning accuracy significantly [4].

A GNSS simulator provides a superior alternative for testing compared to using actual GNSS signals in a live environment. It offers full control over simulated satellite signals and environmental conditions, enabling comprehensive, repeatable tests that would be difficult or impossible with real-world data. Simulators allow testers to precisely generate GNSS signals for any location and time, testing scenarios for any place on Earth or in space, past, present, or future, all within the controlled environment of the laboratory. Additionally, simulators can model vehicle motion, whether for aircraft, ships, spacecraft, or land vehicles, allowing for simulations of various trajectories and vehicle dynamics without the need for physical movement. Moreover, GNSS simulators can simulate a wide range of environmental conditions that impact receiver performance, such as atmospheric disturbances, multi-path reflections, antenna characteristics, and interference. For example, the atmosphere can be completely disabled, or specific atmospheric errors can be applied using known models, allowing testers to analyze the impact of such errors on receiver performance. Similarly, multi-path effects can be completely removed or precisely modeled, enabling researchers to study the effects of multi-path on receivers and apply design adjustments or mitigation techniques [5,6]. This level of control and precision enables targeted tests that focus on specific aspects of receiver performance while isolating others for more detailed analysis. Simulators also allow for precise manipulation of satellite signals, making it possible to test the performance of receivers under conditions that include satellite clock errors, orbital inaccuracies, and signal disruptions. In contrast to real GNSS signals, the signals generated by a simulator are virtually noiseless, offering the best possible signal-to-noise ratio for testing. The signals produced are exactly known and identical, such that the satellite positions and their relative code phases match in the tested scenarios at the same location, time, and date. This repeatability is crucial for assessing receiver performance, as it ensures that the same conditions are applied in every test, allowing for accurate performance evaluation and receiver sensitivity testing [7]. In addition to offering control and repeatability, GNSS simulators provide significant time and cost savings. Since the test conditions such as signal errors are precisely reproducible, measurements can be repeated multiple times under the same circumstances, a feat not possible with real GNSS signals. This scalability of test complexity from basic testing with a single static satellite to advanced simulations involving multi-GNSS systems, atmospheric effects, and multi-path modeling provides a comprehensive environment for testing under any condition [8]. The ability to simulate real-world conditions in a cost-effective and scalable manner highlights the suitability of such a simulator for both research and practical implementations, meeting the demands of modern navigation and positioning systems.

These capabilities support the development of a GLONASS simulator for testing and verifying GNSS receiver performance in research and development, which can be tailored to address similar applications by improving positioning accuracy, assessing the impact of Dilution of Precision (DOP), and evaluating performance under dynamic and high-speed scenarios [5]. DOP quantifies how the distribution of satellites affects the propagation of errors. It represents the geometric arrangement of satellites relative to the GNSS receiver, serving as a direct measure of the quality of satellite geometry and its effect on positional accuracy. A low DOP value signifies an optimal satellite distribution across the sky, which ensures that even small timing errors in signal propagation have minimal impact on the computed position. This condition improves accuracy, as the broad spatial distribution allows the positions more precise [9,10]. In contrast, a high DOP value arises when satellites are closely clustered or poorly spread within the receiver's field of view, typically along a single line or confined plane. Under such unfavorable geometries, any minor discrepancies in signal timing or path delays are magnified, leading to significant errors in the derived

In Press

position. This amplification occurs because the system has fewer geometric baselines to cross-reference, compromising the precision of location estimates [11]. By focusing on reducing DOP, the GNSS simulator can systematically mitigate these geometric vulnerabilities, thereby enhancing the robustness and reliability of positioning solutions [12].

This research presents a GLONASS simulator that takes target receiver motion and time as input, generates GNSS satellites' positions from the ephemeris, and simulates the signals based on visible satellites to be received by the GNSS receiver. The simulator accounts for tropospheric errors in measurements and also can incorporate receiver clock bias. Besides, it focuses on enhancing navigation precision by minimizing the DOP, a pivotal factor in determining the accuracy of GNSS positioning. Through targeted analysis and constellation modifications, the simulator seeks to identify optimal configurations that can reduce DOP and improve positioning reliability. As a further step, after selecting the best constellation enhancement, a virtual satellite is integrated into the system to reduce the DOP value. The added satellite is selected using fuzzy logic in such a way that it minimizes the DOP.

The article structure is as follows: Section 2 refers to proposed modeling the GLONASS satellite signal simulator. The impact of geometric arrangement DOP on pseudo-range calculations and measurement accuracy is examined in Section 3. Section 4 describes the proposed method to generate a GLONASS satellite signal and enhance the accuracy of the simulator. The results and performance evaluation of the proposed method are reviewed in Section 5. Finally, Section 6 provides conclusions and suggestions for future research.

2 Proposed GLONASS Satellite Signal Modeling

The overall structure of the baseband GLONASS simulator is shown in Fig. 1.

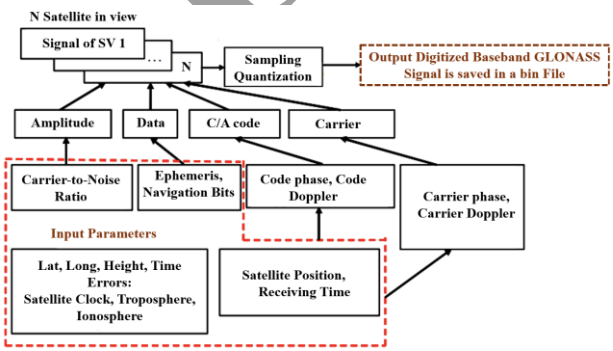

Fig 1. Proposed GLONASS simulator structure.

The following provides a concise description of the blocks related to signal modeling and generation.

2.1 GetVisibleSat

This algorithm provides a critical step in GLONASS signal modeling, enabling the identification of visible satellites at any moment and determining their geometric relationship to the receiver, which is essential for accurate positioning and navigation. The GLONASS ephemeris is loaded from a broadcast ephemeris (BRDC) file obtained from the Crustal Dynamics Data Information System Institute (CDDIS) website. For each satellite, the algorithm estimates its position at the start time by solving Runge–Kutta equations to obtain the satellite's coordinates in the Earth-Centered, Earth-Fixed (ECEF) frame. The next step involves calculating the distance between the receiver and the satellite using the Euclidean distance, which yields the pseudo-range that we will discuss in Section 2.4. The travel time is computed by dividing the pseudo-range by the speed of light, providing the signal propagation time. Because the signal takes some time to travel from the satellite to the receiver antenna, Earth's rotation must be taken into account. The baseband GLONASS simulator uses the receiving time as its reference time. This step adjusts the satellite's transmission time coordinates to their corresponding reception time coordinates, ensuring that the satellite's ECEF position is accurate at the moment the signal is received. Once the corrected position is obtained, the algorithm calculates the satellite's elevation and azimuth angles relative to the receiver's position using topocentric coordinates. This function returns the satellite's azimuth and elevation angles based on the receiver's geographic location. By applying an elevation mask, satellites with elevation angles below the minimum threshold are filtered out. The final list of visible satellites consists of those whose elevation exceeds the masking angle [13–16].

2.2 GenerateCAcode

The provided algorithm generates the GLONASS Coarse/Acquisition (C/A) code based on the satellite's Pseudo-Random Noise (PRN) number, which uniquely identifies each satellite in the constellation. The core of the algorithm relies on generating the maximum-length sequence (M-sequence) using a Linear Feedback Shift Register (LFSR) with a degree-9 polynomial. The C/A code repeats every 1 millisecond, corresponding to a chip rate of 511 kbps. This results in a sequence length of $N = 2^9 - 1 = 511$ bits. The characteristic polynomial for the

In Press

LFSR is $P_x = x^9 + x^4 + 1$. This polynomial determines the feedback taps used to produce the pseudorandom sequence. The initialization vector for the LFSR is '111111111'. At each clock, the new bit is calculated as the modulo-2 (XOR) sum of the feedback taps at stages 9 and 4. The shift register is then updated, and the output bit is appended to the code sequence. This process ensures that the generated C/A code accurately represents the GLONASS signal's pseudorandom sequence, which is crucial for signal synchronization, timing, and positioning in satellite navigation systems [12].

2.3 GenerateNavMsg

The algorithm for generating the GLONASS navigation message begins by determining the reference time, defined as the nearest 30-second interval to the start time. This step ensures that the navigation message is synchronized with the GLONASS satellite's time frame. A fixed 30-bit preamble is then assigned to the beginning of each navigation message to mark the start of the frame and facilitate receiver synchronization. The navigation frame is initialized with 85 bits, each derived from the ephemeris frame data. At this point, a bitstream is also initialized to store the complete navigation message. The algorithm processes the ephemeris data by converting each value into its binary representation. It then computes a checksum (CRC), which is essential for error detection and data integrity. The checksum is calculated by performing a cyclic redundancy check using an XOR operation on the bit-reversed 85-bit string. This operation generates an 8-bit checksum that is appended to each frame to detect any transmission errors that may occur, ensuring the reliability of the navigation data. The next step involves constructing the 15 frames of 85 bits by combining the ephemeris data with its associated 8-bit checksum. Once the 15 frames are generated, they are concatenated into a continuous bitstream, which will be used in the GLONASS transmission process. The bitstream undergoes an encoding procedure using a LFSR, a key component in the modulation and error-correction process for GLONASS signals. The LFSR performs a bitwise XOR operation on the concatenated bitstream, producing an encoded message that is ready for transmission. The final encoded message consists of the original bits of ephemeris bits, the checksum, and the 30-bit preamble arranged in a sequential bitstream format [6].

2.4 ComputeRange

The algorithm for computing the pseudo-range in the GLONASS signal model begins by integrating key parameters, including receiver and satellite positions, clock corrections, and velocity information. The satellite signal travels a specific time interval (Δt) to reach the receiver [13]. As mentioned in Section 2.1, the receiver's reception time serves as the reference for determining the corresponding transmission time. During this interval, both the Earth and the satellite undergo rotational movements. The transmit time is corrected using satellite clock error, relativistic effects, and tropospheric delays. To ensure precise pseudo-range estimation, as outlined in Eq. (1), the relative motion between the Earth and the satellite must be considered. This correction enables an accurate determination of the satellite's position before accounting for Earth's rotation [14]. Fig. 2 illustrates this process.

$$\text{Psudorange} = \text{norm}(\text{satPos} - \text{RxPos}) \quad (1)$$

The satPos vector represents the estimated satellite position, while the RxPos vector denotes the receiver position, both known at a specific time and location. The initial satellite position is extracted from the BRDC file [15], and during the simulation, this position is continuously updated and refined using the 4th-order Runge-Kutta method [16], ensuring robust and accurate pseudo-range estimation. Additionally, clock corrections and relative velocity estimates are calculated to support dynamic modeling. The process of calculating the relative velocity can be summarized in steps (1) and (2):

1. Estimation of the relative vector from the rover (recVel) to a satellite velocity (satVel) which is calculated using Eq. (2) [17]:

$$\text{relaVel} = \text{satVel} - \text{recVel} \quad (2)$$

2. Estimation of the line of sight (LOS) velocity according to Eq. (3):

$$V_{LOS} = \langle \frac{\text{satPos} - \text{RxPos}}{\text{Psudorange}}, \text{relaVel} \rangle \quad (3)$$

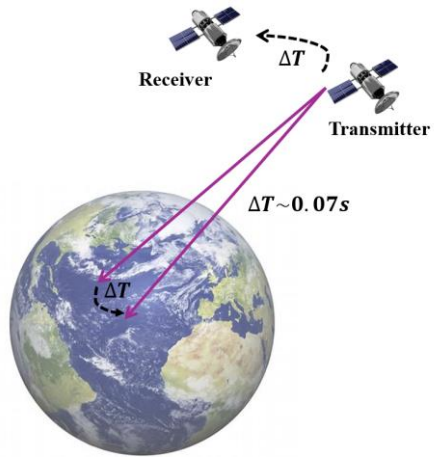

Fig 2. Effect of Earth's rotation.

In Press

2.5 ComputecodePhase

The proposed algorithm focuses on accurately modeling the code phase, carrier phase, and Doppler frequency of GLONASS signals. A general guideline is that a rover moving approximately 100 km will cause a 1º variation in the satellite's elevation. The Doppler frequency shift is influenced by the relative velocity between the satellite and the receiver. According to the model, each GLONASS signal channel has a unique carrier frequency that is shifted around the central frequency based on the channel number. The wavelength of the carrier signal is calculated by dividing the speed of light by the carrier frequency, which incorporates the channel-specific frequency offset and spacing. Next, the Doppler frequency is derived by dividing the relative velocity (V_{LOS}), defined in Section 2.4, by the calculated wavelength. The carrier frequency is then determined by adding the Doppler frequency to the nominal carrier frequency corresponding to the GLONASS channel. Similarly, the code frequency is adjusted based on Doppler variations to maintain synchronization between the carrier and code tracking loops. This adjustment uses a scaling factor derived from the ratio of the nominal code frequency to the nominal carrier frequency. To determine the initial code phase, the algorithm calculates the elapsed time since the reference epoch in milliseconds. The fractional part of this time is used to yield the initial code phase, representing the starting position within one full spreading-code sequence [14].

2.6 SignalGenerating

The signal-generation model aims to replicate realistic GLONASS signal behavior. This model incorporates essential factors such as satellite ephemeris data, receiver position, Doppler shifts, clock biases, and antenna gain patterns. Each of these elements is critical for accurately simulating the signal environment and ensuring that the generated signal behaves consistently with real GLONASS transmissions. To begin, the model computes the position of each GLONASS satellite relative to the receiver's location, using ephemeris data. The positions are updated according to time and receiver motion. This enables precise pseudo-range calculation, as described in Section 2.4. In addition, the model accounts for satellite visibility by applying the receiver's elevation mask. As noted in Section 2.1, only those satellites above the minimum elevation threshold are included. The navigation bits, initialized in Section 2.3, are updated every 30 seconds. As declared in Section 2.5, the Doppler shift is another key component and is computed from the relative velocity between the receiver and each satellite. As the receiver moves relative to the satellite, the frequency of the received signal shifts either upward or downward. This Doppler effect must be incorporated into the simulation, as it affects the perceived frequency of the incoming signal and can influence the accuracy of time synchronization and positioning. The core of the signal generation involves modulating the waveform to emulate the GLONASS transmission structure. In this model, Binary Phase Shift Keying (BPSK) is used, consistent with standard GLONASS modulation. An essential part of the simulation involves modeling the receiver's clock bias. Since the receiver clock is not perfectly synchronized with GNSS time, an offset is always present and must be included in the simulation. This bias is introduced and updated throughout the process, reflecting the real-world challenges of achieving accurate timing and precise position estimation.

Once the individual satellite signals have been modulated, the model combines them into a single composite signal. The resulting waveform is a superposition of all the visible satellites. Furthermore, the model adjusts the signal strength Carrier-to-Noise Ratio (C/N_0) based on the satellite's elevation, atmospheric conditions, and antenna gain pattern. Environmental factors such as ionospheric delays, multipath, and other noise sources are neglected in this study. The final output reflects the complex characteristics of real GLONASS signals. It includes modulations and encoding time shifts due to pseudo-ranges, Doppler shifts, clock biases, and signal attenuation due to distance and environmental factors. The generated signal is produced by integrating the C/A code explained in Section 2.2, navigation bits, and carrier with a C/N_0 value. The simulated signal is quantized via an Analog to Digital Converter (ADC) block. This detailed model enables GLONASS signal simulation under a range of conditions, providing a valuable testbed for evaluating receiver algorithms, assessing performance, and analyzing how signal quality affects positioning accuracy [18-20].

3 Satellite Geometry and Dilution of Precision Modeling

The satellites transmit ranging signals and navigation data, enabling the user to compute pseudo-ranges and estimate positions. The receiver performs several functions, including acquisition, code and carrier tracking, navigation bit extraction, navigation data decoding, pseudo-range estimation, and position computations [21]. During the acquisition stage, rough

In Press

estimates of the signal parameters are obtained, which are then refined through the tracking loops. Once tracking is complete, the navigation data can be extracted, and pseudo-ranges can be calculated [22,23]. An overview of the GNSS receiver is illustrated in the block diagram shown in Fig. 3.

Moreover, to determine the user's three-dimensional position (x_u, y_u, z_u) and the receiver clock bias t_b, pseudo-range measurements are obtained from at least four satellites using Eq. (4) [24]:

$$f(x_u,y_u,z_u,t_b) = \rho_j = \|s_j - u\| + ct_b = \sqrt{(x_j - x_u)^2 + (y_j - y_u)^2 + (z_j - z_u)^2} + ct_b \quad (4)$$

Here, j ranges from 1 to 4 and references the satellite number. x_j, y_j, and z_j represent the three-dimensional coordinates of the jth satellite. By expanding Eq. (4) in a Taylor Series around the approximate position ($\hat{x}_u$, $\hat{y}_u$, $\hat{z}_u$), the displacement vector (Δx_u, Δy_u, Δz_u) can be expressed as linear functions of the known satellite coordinates and pseudo-range measurements. Using the approximate position ($\hat{x}_u$, $\hat{y}_u$, $\hat{z}_u$) and the estimated clock bias $\hat{t}_b$, an approximate pseudo-range can be calculated as Eq. (5) [24,25]:

$$\hat{\rho}_j = \sqrt{(\hat{x}_j - x_u)^2 + (\hat{y}_j - y_u)^2 + (\hat{z}_j - z_u)^2} + c\hat{t}_b = f(\hat{x}_u, \hat{y}_u, \hat{z}_u, \hat{t}_b) \quad (5)$$

As stated earlier, the unknown user position and receiver clock offset are considered to consist of an approximate value and a small incremental correction, as expressed in Eq. (6) [26]:

$$x_u = \hat{x}_u + \Delta x_u,\ y_u = \hat{y}_u + \Delta y_u,\ z_u = \hat{z}_u + \Delta z_u,\ t_b = \hat{t}_b + \Delta t_b \quad (6)$$

Therefore, we can write Eq. (7) [25]:

$$f(x_u,\ y_u,\ z_u, t_b) = f(\hat{x}_u + \Delta x_u,\ \hat{y}_u + \Delta y_u,\ \hat{z}_u + \Delta z_u, \hat{t}_b + \Delta t_b) \quad (7)$$

As mentioned, this function can be expanded around the approximate point and the corresponding estimated receiver clock bias ($\hat{x}_u$, $\hat{y}_u$, $\hat{z}_u$, $\hat{t}_b$) using a Taylor Series as shown in Eq. (8) [26]:

$$(\hat{x}_u + \Delta x_u, \hat{y}_u + \Delta y_u, \hat{z}_u + \Delta z_u, \hat{t}_b + \Delta t_b) = f(\hat{x}_u, \hat{y}_u, \hat{z}_u, \hat{t}_b) + \frac{\partial f(\hat{x}_u,\hat{y}_u,\hat{z}_u,\hat{t}_b)}{\partial \hat{x}_u}\Delta x_u + \frac{\partial f(\hat{x}_u,\hat{y}_u,\hat{z}_u,\hat{t}_b)}{\partial \hat{y}_u}\Delta y_u + \frac{\partial f(\hat{x}_u,\hat{y}_u,\hat{z}_u,\hat{t}_b)}{\partial \hat{z}_u}\Delta z_u + \frac{\partial f(\hat{x}_u,\hat{y}_u,\hat{z}_u,\hat{t}_b)}{\partial \hat{t}_u}\Delta t_u + \cdots \quad (8)$$

The expansion is truncated after the first-order partial derivatives to eliminate non-linear terms. Therefore, the partial derivatives evaluate as shown in Eq. (6) [26]:

$$\frac{\partial f(\hat{x}_u,\hat{y}_u,\hat{z}_u,\hat{t}_b)}{\partial \hat{x}_u} = -\frac{x_j - \hat{x}_u}{\hat{r}_j},\quad \frac{\partial f(\hat{x}_u,\hat{y}_u,\hat{z}_u,\hat{t}_b)}{\partial \hat{y}_u} = -\frac{y_j - \hat{y}_u}{\hat{r}_j},\quad \frac{\partial f(\hat{x}_u,\hat{y}_u,\hat{z}_u,\hat{t}_b)}{\partial \hat{z}_u} = -\frac{z_j - \hat{z}_u}{\hat{r}_j},\quad \frac{\partial f(\hat{x}_u,\hat{y}_u,\hat{z}_u,\hat{t}_b)}{\partial \hat{t}_u} = c \quad (9)$$

Where $\hat{r}_j = \sqrt{(\hat{x}_j - x_u)^2 + (\hat{y}_j - y_u)^2 + (\hat{z}_j - z_u)^2}$.

Substituting Eq. (8) and Eq. (9) into Eq. (8) yields Eq. (10) [25,27]:

$$\rho_j = \hat{\rho}_j - \frac{x_j - \hat{x}_u}{\hat{r}_j}\Delta x_u - \frac{y_j - \hat{y}_u}{\hat{r}_j}\Delta y_u - \frac{z_j - \hat{z}_u}{\hat{r}_j}\Delta z_u + ct_b \quad (10)$$

Eq. (4) has now been linearized with respect to the unknowns Δx_u, Δy_u, Δz_u, and Δt_b [26]. By rearranging the resulting expression to place the known quantities on the left-hand side and the unknowns on the right-hand side, we obtain Eq. (11) [27]:

$$\Delta\rho = \hat{\rho}_j - \rho_j = \frac{x_j - \hat{x}_u}{\hat{r}_j}\Delta x_u + \frac{y_j - \hat{y}_u}{\hat{r}_j}\Delta y_u + \frac{z_j - \hat{z}_u}{\hat{r}_j}\Delta z_u - ct_b \quad (11)$$

Where $a_{x_j} = \frac{x_j - \hat{x}_u}{\hat{r}_j}$, $a_{y_j} = \frac{y_j - \hat{y}_u}{\hat{r}_j}$, and $a_{z_j} = \frac{z_j - \hat{z}_u}{\hat{r}_j}$ denote the direction cosines of the unit vector pointing from the approximate user position to the jth satellite. We now have four unknowns: Δx_u, Δy_u, Δz_u, and Δt_b, which can be determined using pseudo-range measurements from four satellites. These unknowns are obtained by solving the set of linear equations in Eq. (12) [27,28]:

$$\Delta\rho = \begin{bmatrix}\Delta\rho_1\\ \Delta\rho_2\\ \Delta\rho_3\\ \Delta\rho_4\end{bmatrix}, H = \begin{bmatrix}ax_1 & ay_1 & az_1 & 1\\ ax_2 & ay_2 & az_2 & 1\\ ax_3 & ay_3 & az_3 & 1\\ ax_4 & ay_4 & az_4 & 1\end{bmatrix}, \Delta x = \begin{bmatrix}\Delta x_u\\ \Delta y_u\\ \Delta z_u\\ -c\Delta t_b\end{bmatrix} \quad (12)$$

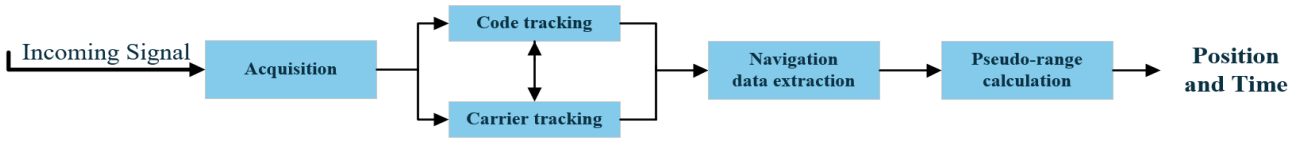

Fig 3. Receiver block diagram.

In Press

One obtains, finally Eq. (13) [27]:

$$\Delta\rho = H\Delta x \quad (13)$$

Which has the solution Eq. (14) [27]:

$$\Delta x = H^{-1}\Delta\rho \quad (14)$$

Once the unknowns are computed, the user's coordinates x_u, y_u, z_u and the receiver clock offset t_b are calculated using Eq. (6). This linearization approach is valid as long as the displacement (Δx_u, Δy_u, Δz_u) remains close to the linearization point. The acceptable displacement depends on the user's accuracy requirements. If the displacement exceeds this threshold, the process is repeated, with $\hat{\rho}$ replaced by a new pseudo-range estimate based on the updated coordinates x_u, y_u, and z_u [26,27]. The least square solution can be formally obtained by multiplying both sides of Eq. (13) on the left by the transpose of the matrix H, yielding $H^T H\Delta x = H^T\Delta\rho$. The matrix product $H^T H$ is a 4 × 4 square matrix, and the unknown vector Δx can be solved by multiplying both sides by the inverse, $(H^T H)^{-1}$ as shown in Eq. (15) [26].

$$\Delta x = (H^T H)^{-1} H^T \Delta\rho \quad (15)$$

This represents the least-squares formulation for Δx as a function of $\Delta\rho$. It can be noted that if n = 4, $(H^T H)^{-1} = H^{-1}(H^T)^{-1}$ and Eq. (15) simplifies to Eq. (14). The pseudo-range measurements are not error-free and can be expressed as a linear combination of three components, as shown in Eq. (16) [27]:

$$\Delta\rho = \rho_T - \rho_L + d\rho \quad (16)$$

Where, ρ_T is the vector of error-free pseudo-range values, ρ_L is the vector of pseudo-range values computed at the linearization point, and $d\rho$ represents the net error in the pseudo-range values. Similarly, Δx can be expressed as Eq. (17):

$$\Delta x = x_T - x_L + dx \quad (17)$$

Where x_T is the error-free position and time, x_L is the position and time defined as the linearization point, and dx is the error in the position and time estimate. By substituting Eq. (16) and Eq. (17) into Eq. (15) and using the relation $x_T - x_L = (H^T H)^{-1} H^T(\rho_T - \rho_L)$ which follows from $H(x_T - x_L) = (\rho_T - \rho_L)$, a restatement of Eq. (13), we obtain Eq. (18) [26]:

$$dx = [(H^T H)^{-1} H^T] d\rho = K d\rho \quad (18)$$

The matrix K is defined by the expression in brackets. Eq. (18) describes the functional relationship between errors in the pseudo-range measurements and the resulting errors in the computed position and receiver clock bias. It is valid provided that the linearization point is sufficiently close to the user's location and that the pseudo-range errors are small enough so that the error in performing the linearization can be ignored. Eq. (18) represents the fundamental relationship between pseudo-range errors and the resulting errors in the estimated position and clock bias. The matrix $(H^T H)^{-1} H^T$, sometimes called the least-squares solution matrix, is a 4 × n matrix that depends only on the relative geometry of the user and the satellites used in the least-squares computation. In many applications, the user/satellite geometry can be considered fixed, and Eq. (18) then establishes a linear relationship between the pseudo-range errors and the induced position and time bias errors [25]. The pseudo-range errors are treated as random variables, and Eq. (18) expresses dx as a random variable functionally related to $d\rho$. The error vector $d\rho$ is usually assumed to have jointly Gaussian, zero-mean components. With the geometry considered fixed, dx is also Gaussian and zero-mean [28]. The covariance of dx is obtained by forming the product $dx dx^T$ and computing an expected value. By definition, Eq. (19) expresses this relationship as:

$$cov(dx) = E[dx dx^T] \quad (19)$$

Where Eq. (19) denotes the covariance of dx and E represents the expectation operator. Substituting from Eq. (18) and viewing the geometry as fixed, Eq. (20) obtains [5,26]:

$$cov(dx) = E[K d\rho k \rho^T K^T] = E[(H^T H)^{-1} H^T d\rho d\rho^T H (H^T H)^{-1}] = (H^T H)^{-1} H^T cov(d\rho)(H^T H)^{-1} \quad (20)$$

Note that in this computation, $(H^T H)^{-1}$ is symmetric. This follows from the general matrix relations $(AB)^T = B^T A^T$ and $(A^{-1})^T = (A^T)^{-1}$, which hold whenever the operations are defined It is commonly assumed that the components of $d\rho$ are identically distributed and independent, with variance equal to the square of the satellite User-Equivalent Range Error (UERE). Under these assumptions, the covariance of $d\rho$ is a scalar multiple of the identity matrix, as shown in Eq. (21) [24-28]:

$$cov(d\rho) = I_{n*n}\delta^2_{UERE} \quad (21)$$

The value δ^2_{UERE} is the pseudo-range error factor and I_{n*n} is the n × n identity matrix. Substitution this into Eq. (20) yields Eq. (22) [24]:

$$cov(dx) = (H^T H)^{-1}\delta^2_{UERE} \quad (22)$$

Under the stated assumptions, the covariance of the errors in the computed position and receiver clock bias is

In Press

a scalar multiple of the matrix $(H^T H)^{-1}$. The vector dx has four components, representing the errors in the estimated values of $x_T = (x_u, y_u, z_u, ct_b)$. The covariance of dx is a 4 × 4 matrix and can be expressed in the expanded form as shown in Eq. (23) [5,23]:

$$cov(dx) = \begin{bmatrix} \delta^2_{x_u} & \delta^2_{x_u,y_u} & \delta^2_{x_u,z_u} & \delta^2_{x_u,ct_b} \\ \delta^2_{x_u,y_u} & \delta^2_{y_u} & \delta^2_{y_u,z_u} & \delta^2_{y_u,ct_b} \\ \delta^2_{x_u,z_u} & \delta^2_{y_u,z_u} & \delta^2_{z_u} & \delta^2_{z_u,ct_b} \\ \delta^2_{x_u,ct_b} & \delta^2_{y_u,ct_b} & \delta^2_{z_u,ct_b} & \delta^2_{ct_b} \end{bmatrix} \quad (23)$$

The components of the matrix $(H^T H)^{-1}$ indicate how pseudo-range errors propagate into the covariance of dx. Dilution of precision parameters in GLONASS is defined as the ratios of specific combinations of the components of $cov(dx)$ and δ^2_{UERE}. The DOP definitions implicitly assume that the user/satellite geometry is considered fixed [29]. Additionally, it is assumed that local user coordinates are used to specify $cov(dx)$ and dx. The positive x-axis points east, the y-axis points north, and the z-axis points up. The most general parameter, termed the Geometric Dilution of Precision (GDOP), is defined by Eq. (24) [28]:

$$GDOP = \frac{\sqrt{\delta^2_{x_u} + \delta^2_{y_u} + \delta^2_{z_u} + \delta^2_{ct_b}}}{\delta^2_{UERE}} \quad (24)$$

3.1 Impact of DOP on Pseudo-Range Calculations and Measurement Accuracy

To illustrate the concept of DOP in GNSS systems such as GLONASS, consider a classic example: determining position using signals from two distinct sources, such as foghorns [30]. In this scenario, a user estimates their position based on range measurements from two foghorn signals. Assuming the user has a synchronized time base relative to the foghorns and precise information about their locations and transmission times, the user can measure the Time of Arrival (TOA) of each signal to compute the propagation time. This allows the user to determine their distance from each foghorn, ultimately estimating their position by identifying the intersection of the range circles derived from the TOA measurements [25,26].

In the presence of measurement errors, the range rings used to determine the user's position will be inaccurate, resulting in errors in the computed position. This is where the concept of DOP becomes crucial [22]: DOP quantifies the impact of the geometric constellation of the signal sources relative to the user on the final positioning error. Essentially, the degree of DOP depends on the spatial distribution of these sources [31-33]. In Fig. 4a, the foghorns are positioned at nearly right angles relative to the user, providing an optimal constellation that minimizes positional error ($\boldsymbol{\varepsilon}$). By contrast, in Fig. 4b, the foghorns are aligned at a smaller angle from the user's perspective, resulting in a less favorable geometric constellation. In both figures, the error-free range circles intersect precisely at the user's location. However, the additional segments around these circles illustrate how ranging errors can affect the calculated position. While the range error in both cases is identical, the shaded areas indicate the possible range of user positions based on these error margins [34]. Notably, even with the same measurement error, the geometry in Fig. 4b produces a larger potential positional error, as indicated by the wider shaded region. This difference arises due to the concept of DOP: the more favorable geometry in Fig. 4a yields a lower DOP, minimizing the impact of ranging errors, whereas the geometry in Fig. 4b corresponds to a higher DOP, amplifying positional errors. Consequently, for similar measurement inaccuracies, constellations with lower DOP, like that in Fig. 4a, provide greater accuracy in the computed positions. This example highlights the importance of DOP optimization in satellite positioning, as an effective geometric distribution of satellites can significantly reduce error margins in critical applications [29, 35-38].

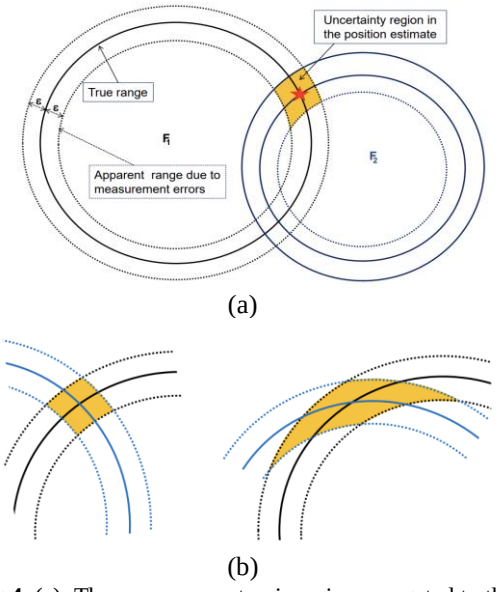

Fig 4. (a): The measurement noise ε is propagated to the position estimate as an uncertainty region, and (b): The DOP effect in positioning: a 2D illustration showing how the uncertainty region varies with geometry [24].

4 Proposed GLONASS Signal Simulator to Enhance Accuracy

This section describes the structure of the GLONASS signal simulator. Fig. 5 illustrates the process of generating GLONASS satellite signal data. The simulator takes four primary inputs: longitude, latitude, altitude, and time. Given the half-hour update rate of the BRDC file [15], 48 satellite constellations are generated throughout the day. The appropriate ephemeris is determined based

In Press

on the simulation time. The t_k and t_b time parameters in the subframes are extracted from the user-defined time to ensure alignment between the simulation and the current time. Here, t_k represents the time referenced to the beginning of the frame within the current day, while t_b serves as an index for a specific time interval within the day, according to UTC(SU) + 03:00 hours [34].

In the next step, the satellites in the LOS are identified and chosen based on the selected simulation time. The GLONASS signal generator starts the simulation based on the number of visible satellites and the specified duration.

According to the explanations provided in Section 2, The baseband signal is generated by the product of the C/A code samples, navigation bits, local carrier, and C/N_0. After quantizing, finally, the baseband signal is SDR transmitted to the target receiver in the RF band by the transmitter Universal Software Radio (USRP). In addition, to improve the accuracy of the simulator, two scenarios are proposed in this paper, which will be discussed in the following sections 4.1 and 4.2.

4.1 Optimization of Satellite Constellation: Minimizing GDOP using Moving Average

As mentioned, there are 48 different satellite constellations throughout 24-hours. As discussed in Section 2, reducing the DOP leads to improved positioning accuracy for the receiver. Therefore, the first scenario focuses on selecting the optimal DOP. To achieve this, the minimum GDOP over the 24 hours is extracted as the best satellite constellation [34,39,40]. The Moving Average (MA) strategy [41], with a window size of 3, is used to identify the best local satellite constellation. The moving average calculates the mean of data points within a fixed window that slides across the dataset. For updating the average, as the window shifts, whole data points are involved, ensuring the average dynamically reflects as Eq. (25). Fig. 6 illustrates the diagram of this algorithm.

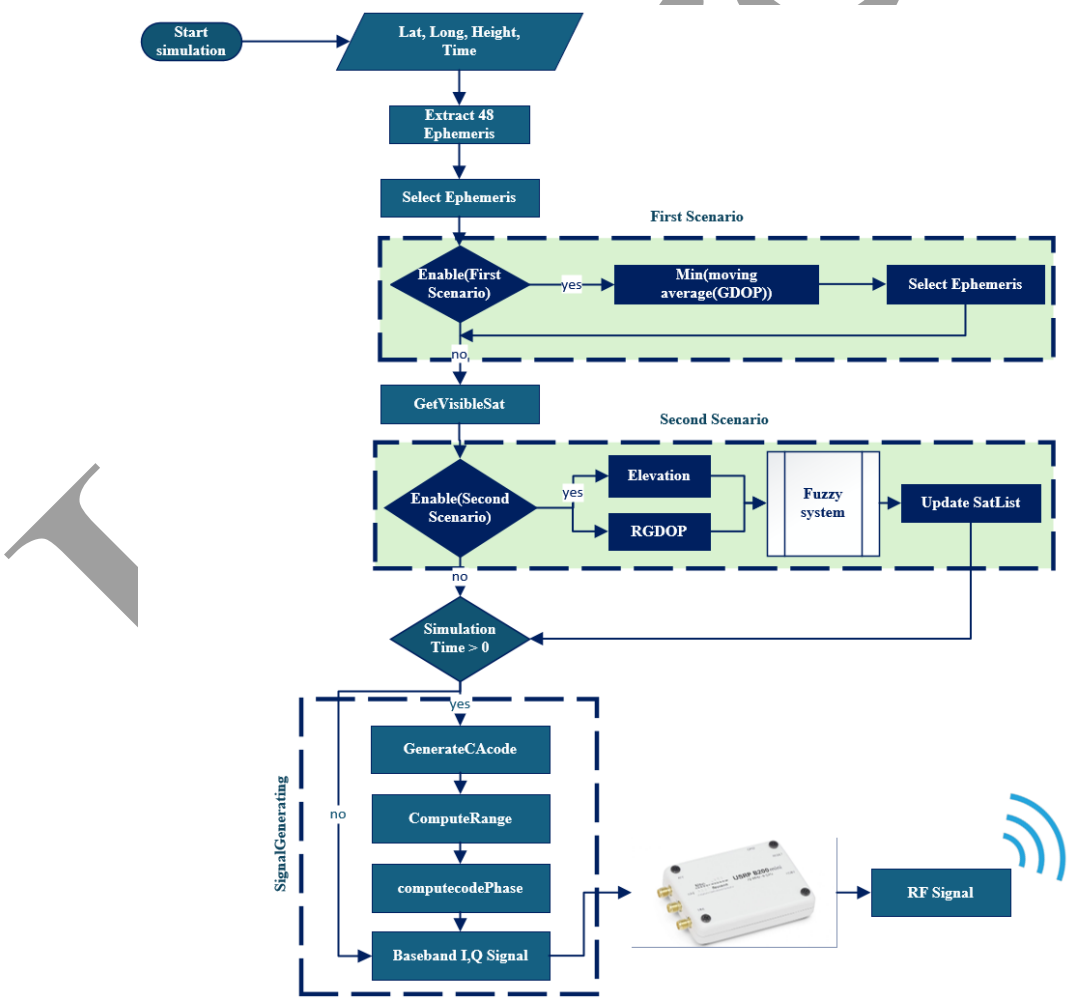

Fig 5. Block diagram of proposed GLONASS signal simulator.

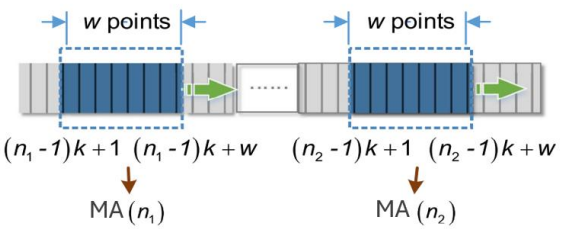

Fig 6. Moving average algorithm.

$$MA = \frac{1}{w}\sum_{i=(n-1)k+1}^{(n-1)k+w} x(i) \quad (25)$$

In which, $x(i)$ represents the ith DOP, w denotes the length of the MA window, k is the sliding step size, and n is the total number of windows. By applying the stated algorithm, the optimal available constellation that makes GDOP minimum over 24 hours is extracted.

4.2 Optimization of Satellite Constellation: Residual Geometric Dilution of Precision (RGDOP) and Fuzzy Logic

The DOP metric serves as an appropriate criterion for evaluating the precision of positioning. However, this metric is defined for a set of satellites and cannot be directly used to assess individual satellites. As a result, it becomes essential to define a new metric that can be computed separately for each satellite. In this regard, if the influence of excluding each satellite from the group on the DOP value is considered as a basis for weighting, satellites whose exclusion leads to a significant increase in the DOP will be assigned higher weights. This method ultimately facilitates the selection of the most optimal satellite geometric constellation [39]. In [42], this metric is introduced as Residual Dilution of Precision (RDOP) and is defined for each satellite by the following Eq. (26). This novel approach offers an innovative way to assign weights to satellites.

$$RGDOP_n = \frac{DOP_{total-n}}{DOP_{total}} \quad (26)$$

As shown in Eq. (26), if the removal of the nth satellite leads to a substantial increase in the DOP value for the remaining satellite constellation, the RDOP value for that satellite will be high as well. This suggests that the satellite is crucial in creating an optimal geometric constellation (i.e., satellites with greater spatial separation). Consequently, a higher weight should be attributed to such a satellite.

In the proposed method, the enhanced fuzzy weighted logic approach [43] employs two essential inputs: (1) the RGDOP parameter, and (2) the Elevation angle. The RGDOP parameter, derived from the geometric accuracy adjustment metric, indicates the contribution of each satellite in establishing an optimal geometric constellation, highlighting its significance in improving positioning accuracy. The elevation angle, in contrast, reflects the quality of the transmitted signal and serves as a crucial factor in evaluating the satellite's usability. By incorporating these two inputs into the fuzzy system, the method effectively assigns appropriate weights to each satellite, thereby improving the overall accuracy and reliability of the navigation solution. Based on the variation ranges of the elevation angle and RGDOP, membership functions were defined, as shown in Fig. 7. The membership function for RGDOP is Gaussian and consists of four ranges: very small, small, medium, and large. For the elevation angle, a triangular membership function with three ranges: (1) small, (2) medium, and (3) large was selected. It is important to note that the type and number of membership functions were determined through experimentation. Due to the different impacts of the two inputs, the membership functions for both inputs are applied with varying weights.

Based on the defined membership functions, twelve fuzzy rules were created for the system. As previously noted, a higher elevation angle leads to a higher weight being assigned to the satellite. Similarly, a larger RGDOP signifies the satellite's greater contribution to forming an optimal geometric constellation. The allowable range for the output weights is between 0 and 1. Using this algorithm, the satellite with the highest score is added to the constellation as a virtual satellite in the second scenario, to enhance positioning accuracy. As a result, the following rules were established in Table 1.

5 Numerical Results and Analysis of the Proposed Method

The GLONASS satellite signal simulator is capable of generating various scenarios at arbitrary times and coordinates. Fig. 8 shows the basic operation of the proposed simulator. A GLONASS receiver was used in order to validate each step of the simulator realization. The corroborating results showed that a correct implementation of the GLONASS signal simulator was successfully achieved.

In Press

Table 1. Fuzzy if-then rules determined for proposed fuzzy acquisition algorithm.

	Input membership functions		Output membership function
Rule number	Elevation	RGDOP	SatList threshold
Rule 1	Small	Very Small	Negative Small
Rule 2	Small	Small	Small
Rule 3	Small	Medium	Negative Medium
Rule 4	Small	Large	Positive Small
Rule 5	Medium	Very Small	Small
Rule 6	Medium	Small	Negative Medium
Rule 7	Medium	Medium	Medium
Rule 8	Medium	Large	Positive Medium
Rule 9	Large	Very Small	Positive Small
Rule 10	Large	Small	Positive Medium
Rule 11	Large	Medium	Large
Rule 12	Large	Large	Positive Large

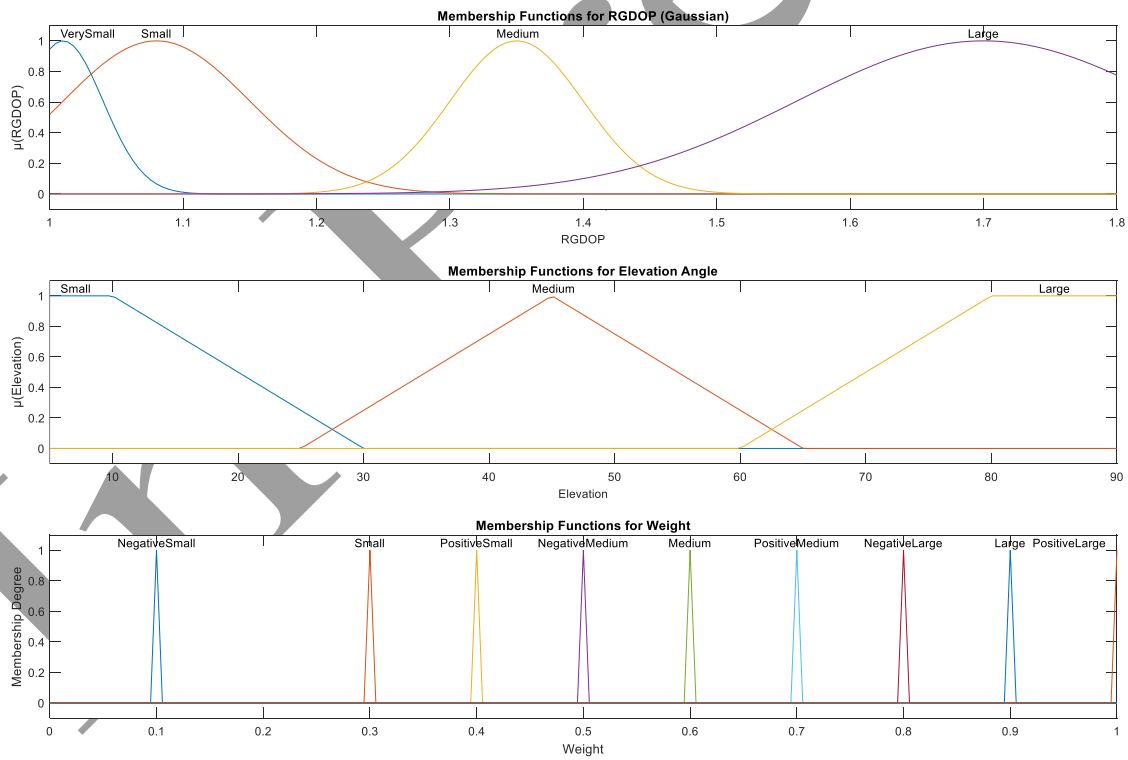

Fig 7. Overall structure of the proposed fuzzy system.

In Press

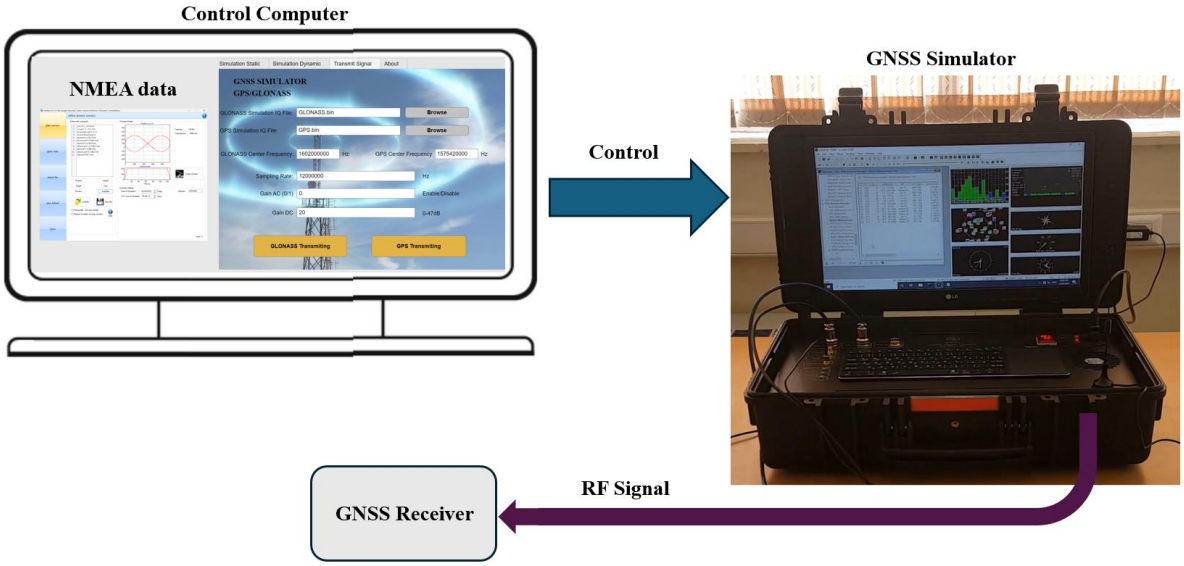

Fig 8. Schematic of the proposed simulator implementation.

As mentioned, the geometric arrangement of satellites is one of the factors affecting the accuracy of calculations related to the pseudo-range and position of the target receiver. The algorithms presented in this paper include intelligent selection of the best DOP during the day and in the second step, adding a virtual satellite using a weighted fuzzy algorithm to reduce the DOP and improve the receiver positioning. This section evaluates the results of the proposed method. The criterion for this evaluation is the accuracy of the receiver position in different scenarios. Table 2 shows some of the features of the simulator.

Table 2. Simulator characteristics.

Center frequency	1602 MHz
Sampling frequency	9 MHz
Intermediate frequency	0
Frequency channel	[-7,6]
Frequency spacing	562.5 kHz
Code frequency	511kHz
update rate	1 kHz
Simulator accuracy	< 50 meters
Signal to noise (SNR)	55 dB
Simulation mode	Static/Dynamic
Elevation mask	20°
Quantization levels	8
Maximum simulation time	24 hours
Speed of light	299792458 m/s

The arbitrary simulation location has been set to the Electrical Faculty at Iran University of Science and Technology in a static mode. The test duration for the example scenario was 30 minutes, corresponding to one complete frame of the BRDC navigation file, with the capability to extend the simulation up to 24 hours. As discussed earlier, the best constellation with minimum DOP is selected in the first step. After applying the first scenario, the satellite constellation geometry is shown in Fig. 9 which includes 7 satellite LOS channels. In the second scenario, the constellation of Fig. 9 is updated by adding a virtual satellite PRN = 7. Under the second scenario, the number of visible satellites increases to 8.

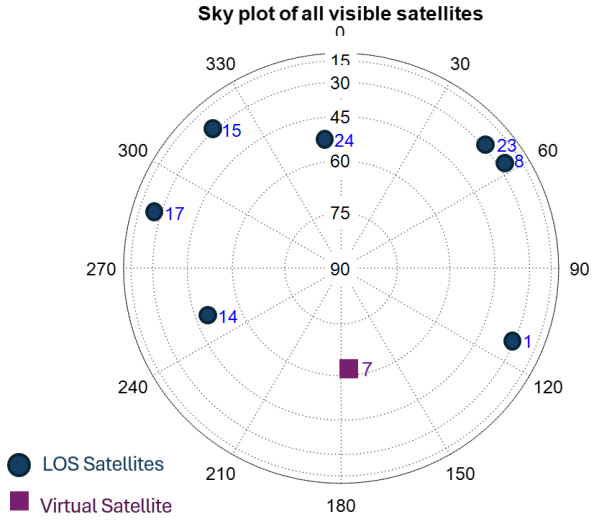

Fig 9. Sky Plot of visible satellites by applying the first and second scenarios of the proposed method.

Table 3 shows the GDOP of the satellites after solving the navigation equations in the receiver under normal conditions, applying the first scenario, and implementing the second scenario.

In Press

Table 3. Simulator capability.

GDOP Value	Normal Condition	First Scenario	Second Scenario
	3.5823	3.2758	2.3875

As can be seen, the proposed algorithm is capable of reducing the GDOP. The proposed approach identifies the satellite that provides the minimum GDOP by achieving the highest score from the rules of Table 1. Table 4 shows the results of the weighted fuzzy algorithm proposed.

Table 4. Virtual satellite selection based on the proposed weighted fuzzy algorithm's scoring.

PRN	Elevation	RGDOP	Fuzzy score
2	33.2304412781519	1.087684069611	0.49220
3	24.4631823194601	1.259259259259	0.27123
4	52.3809087825601	1.117948717948	0.49982
5	56.6753337117228	1.327358490566	0.60604
6	30.8509643241989	1.218220918866	0.52067
7	**62.9672995326147**	**1.372050251256**	**0.73016**
9	43.6335215060459	1.319154113557	0.60255
10	71.0239736498985	1.213472609099	0.71526
11	34.8753286475858	1.122833458929	0.49992
12	20.1179937680987	1.087719298245	0.10004
13	39.9786521023959	1.068965517241	0.4838
18	69.3275823195472	1.201868613138	0.70683
19	49.9420990096428	1.244078794901	0.56624
20	22.7410223503115	1.041095890410	0.10001
21	54.0340504162469	1.178176545223	0.50123

The algorithm searches through all 48 constellations, selecting the non-LOS satellite with the highest score from each constellation to be added as a virtual satellite. Among these virtual satellites, the one with the maximum fuzzy system score is chosen to minimize GDOP. For instance, the results are shown for only one constellation. In this example, satellite PRN 7 is elected with a maximum score of 0.73016.

Table 5 presents a comparison of the error reduction and efficiency of the proposed algorithm under three simulation scenarios: the normal scenario, the first proposed scenario, and the second proposed scenario, with accuracy improvement reported in meters based on the RMSE position error. The results demonstrate a significant improvement in positioning accuracy with the application of the proposed scenarios. Specifically, the error reduction achieved with the implementation of Scenario 1 is 24.4%, while Scenario 2 further improves the accuracy, resulting in a 54.9% error reduction. These findings highlight the effectiveness of the proposed algorithm in enhancing positioning performance.

Table 5. The performance of the proposed spoofing mitigation technique on a static scenario that is reported in meters.

	RMSX (m)	RMSY (m)	RMSZ (m)	RMS (m)
Normal mode	32.45	23.74	28.81	49.46
Scenario 1	25.63	18.97	19.54	37.39
Scenario 2	16.22	12.78	8.40	22.29

6 Conclusions and Future Research

Given the critical role of optimal DOP in improving navigation accuracy, this work presents a GLONASS satellite simulator aimed at optimizing the constellation's GDOP. After proposing modeling and signal generation, two scenarios: (1) identifying the minimal DOP throughout the day, and (2) adding a virtual satellite based on a fuzzy system to further optimize DOP are suggested. To validate and evaluate the proposed method, positioning errors at the receiver were analyzed. The results show that selecting the minimal DOP during the day and incorporating a virtual satellite led to accuracy improvements of 24.4% and 54.9%, respectively. For future research, accuracy can be also enhanced by using Keplerian equation estimations instead of Runge-Kutta, as seen in GPS systems, to predict satellite motion while accounting for Lunar and Solar effects for more precise orbit determination. Additionally, evolutionary algorithms based on artificial intelligence methods can be utilized to predict satellite trajectories with reduced error. Combining and integrating the GLONASS system with other navigation systems, such as GPS, or auxiliary sensors like Inertial Measurement Units (IMUs), can also contribute to further improving navigation accuracy.

Author Contributions

N. Dabaghi Daryan: Conceptualization, Methodology, Software Development, Data Curation, Visualization, Investigation, and Writing, Original Draft.

M. R. Mosavi, S. Mirzakuchaki, and S. Tohidi: Conceptualization, Methodology, Investigation, Supervision, Review & Editing.

In Press

Funding

No funding was received for this work.

Informed Consent Statement

Not applicable.

References

[1]. P. Bethi, S. Pathipati, and P. Aparna, "GNSS Intentional Interference Mitigation via Average KF Innovation and Pseudo Track Updation," 2020 IEEE 17th India Council International Conference (INDICON), pp. 1-5, 2020.

[2]. N. El-Sheimy and Z. Lari, "GNSS Applications in Surveying and Mobile Mapping," Position, Navigation, and Timing Technologies in the 21st Century: Integrated Satellite Navigation, Sensor Systems, and Civil Applications, vol. 2, pp. 1711-1733, 2020.

[3]. L. Chen, F. Zheng, X. Gong, and X. Jiang, "GNSS High-Precision Augmentation for Autonomous Vehicles: Requirements, Solution, and Technical Challenges," Remote Sensing, vol. 15, no. 6, p. 1623, 2023.

[4]. J. Vargas, S. Alsweiss, O. Toker, R. Razdan, and J. Santos, "An Overview of Autonomous Vehicles Sensors and Their Vulnerability to Weather Conditions," Sensors, vol. 21, no. 16, p. 5397, 2021.

[5]. P. Verma, K. Hajra, P. Banerjee, and A. Bose, "Evaluating PDOP in Multi-GNSS Environment," IETE Journal of Research, vol. 68, no. 3, pp. 1705-1712, 2022.

[6]. I. Petrovski, T. Tsujii, J. M. Perre, B. Townsend, and T. Ebinuma, "GNSS Simulation: A User's Guide to the Galaxy," Inside GNSS, vol. 5, no. 5, pp. 52–61, 2010.

[7]. J. Kaivosoja and R. Linkolehto, "GNSS Error Simulator for Farm Machinery Navigation Development," Computers and Electronics in Agriculture, vol. 119, pp. 166-177, 2015.

[8]. X. Yin, Y. Kou, and Z. Zhang, "Design and Implementation of a Flexible Software-Based GNSS IF Signal Simulator," Proceedings of the 22nd International Technical Meeting of the Satellite Division of the Institute of Navigation (ION GNSS 2009), pp. 2229-2240, 2009.

[9]. P. Banerjee, A. Bose, and B. S. Mathur, "A Study on GPS PDOP and Its Impact on Position Error," Indian J. Radio Space Phys., vol. 26, no. 2, pp. 107-111, 1997.

[10]. P. Falkowski-Gilski and Z. Lubniewski, "DOP and Pseudo-Range Error Estimation in Urban Environments for Mobile Android GNSS Applications," WEBIST, pp. 629-638, 2021.

[11]. A. Tabatabaei and M. R. Mosavi, "Rapid and Precise GLONASS GDOP Approximation using Neural Networks," Wireless Personal Communications, vol. 77, pp. 2675-2685, 2014.

[12]. M. Kim, J. Park, G. Jo, and H. Yoo, "Area-Efficient Universal Code Generator for Multi-GNSS Receivers," Electronics, vol. 10, no. 20, p. 2485, 2021.

[13]. P. K. Enge, "The Global Positioning System: Signals, Measurements, and Performance," International Journal of Wireless Information Networks, vol. 1, pp. 83-105, 1994.

[14]. S. Gaglione, A. Angrisano, G. Pugliano, U. Robustelli, R. Santamaria, and M. Vultaggio, "A Stochastic Sigma Model for GLONASS Satellite Pseudo-range," Applied Geomatics, vol. 3, pp. 49-57, 2011.

[15]. A. E. Zinoviev, "Using GLONASS in Combined GNSS Receivers: Current Status," in Proceedings of the 18th International Technical Meeting of the Satellite Division of the Institute of Navigation (ION GNSS 2005), pp. 1046-1057, 2005.

[16]. A. A. Abedi, M. R. Mosavi, and K. Mohammadi, "Low Computational Complexity in Low-Cost GNSS Receivers," Wireless Personal Communications, vol. 112, pp. 37-59, 2020.

[17]. E. G. W. Peters and C. R. Benson, "A Doppler Correcting Software Defined Radio Receiver Design for Satellite Communications," IEEE Aerospace and Electronic Systems Magazine, vol. 35, no. 2, pp. 38-48, 2020.

[18]. D. S. Pecheritsa, S. Yu. Burtsev, and A. A. Frolov, "Method for Determining the Fractional Part of the Cycle of the Carrier Frequency of the Navigation Signal of the GNSS Signal Simulator," Measurement Techniques, vol. 63, no. 11, pp. 891-898, 2021.

[19]. Z. Bo, L. Guang-bin, L. Dong, and F. Zhi-liang, "Real-Time Software GNSS Signal Simulator Accelerated by CUDA," 2010 IEEE 2nd International Conference on Future Computer and Communication, vol. 1, pp. V1-100, 2010.

[20]. O. Julien, B. Zheng, L. Dong, and G. Lachapelle, "A Complete Software-Based IF GNSS Signal Generator for Software Receiver Development," in Proceedings of the 17th International Technical

In Press

Meeting of the Satellite Division of The Institute of Navigation (ION GNSS 2004), pp. 2146–2157, 2004.

[21]. S. Tohidi and M. R. Mosavi, "Fuzzy-Based Acquisition in GPS Receivers for Spoofing Mitigation," Microprocessors and Microsystems, vol. 101, p. 104886, 2023.

[22]. L. Cheng, Y. Dai, W. Guo, and J. Zheng, "Structure and Performance Analysis of Signal Acquisition and Doppler Tracking in LEO Augmented GNSS Receiver," Sensors, vol. 21, no. 2, p. 525, 2021.

[23]. N. Dabaghi Daryan, S. Tohidi, and M. R. Mosavi, "Intelligent Mitigation of GPS Spoofing using the Kalman Filter in the Tracking Loop Based on Multi-Correlator," Survey Review, pp. 1-21, 2024.

[24]. R. B. Langley, "Dilution of Precision," GPS World, vol. 10, no. 5, pp. 52-59, 1999.

[25]. M. R. Mosavi, S. Azarshahi, I. Emamgholipour, and A. A. Abedi, "Least Squares Techniques for GPS Receivers Positioning Filter using Pseudo-Range and Carrier Phase Measurements," Iranian Journal of Electrical and Electronic Engineering, vol. 10, no. 1, pp. 18-26, 2014.

[26]. D. Jwo, "Efficient DOP Calculation for GPS with and without Altimeter Aiding," The Journal of Navigation, vol. 54, no. 2, pp. 269-279, 2001.

[27]. R. O. Nielsen, "Relationship Between Dilution of Precision for Point Positioning and for Relative Positioning with GPS," IEEE Transactions on Aerospace and Electronic Systems, vol. 33, no. 1, pp. 333-338, 1997.

[28]. Y. Teng and J. Wang, "A Closed-Form Formula to Calculate Geometric Dilution of Precision (GDOP) for Multi-GNSS Constellations," GPS Solutions, vol. 20, pp. 331-339, 2016.

[29]. K. N. Ashok, P. S. Kumar, M. K. Mohiddin, M. T. Gemeda, and A. Mishra, "GPS Receiver Position Estimation and DOP Analysis using a New Form of the Observation Matrix Approximations," Journal of Sensors, pp. 1-12, 2022.

[30]. H. Wang, H. Jiang, J. Ou, B. Sun, S. Zhong, M. Song, and A. Guo, "Anomaly Analysis of 18 Years of Newly Merged GPS Ephemeris from Four IGS Data Centers," GPS Solutions, vol. 22, pp. 1-13, 2018.

[31]. M. Tahsin, S. Sultana, T. Reza, and M. Hossam-E-Haider, "Analysis of DOP and Its Preciseness in GNSS Position Estimation," 2015 IEEE International Conference on Electrical Engineering and Information Communication Technology (ICEEICT), pp. 1-6, 2015.

[32]. M. Rychlicki, Z. Kasprzyk, and A. Rosiński, "Analysis of Accuracy and Reliability of Different Types of GPS Receivers," Sensors, vol. 20, no. 22, p. 6498, 2020.

[33]. B. Li, K. Zhao, and X. Shen, "Dilution of Precision in Positioning Systems using Both Angle of Arrival and Time of Arrival Measurements," IEEE Access, vol. 8, pp. 192506-192516, 2020.

[34]. J. Jang, S. Sung, and Y. J. Lee, "Improvement of Differential GPS Performance using Range Measurements Between Satellites," International Journal of Aeronautical and Space Sciences, vol. 21, pp. 201-209, 2020.

[35]. C. Meneghini and C. Parente, "Temporal Analysis of GDOP to Quantify the Benefits of GPS and GLONASS Combination on Satellite Geometry," International Journal of Advanced Computer Science and Applications, vol. 11, no. 3, 2020.

[36]. Y. Teng and J. Wang, "New Characteristics of Geometric Dilution of Precision (GDOP) for Multi-GNSS Constellations," The Journal of Navigation, vol. 67, no. 6, pp. 1018-1028, 2014.

[37]. B. Yan, Y. Li, W. Guo, and Y. Hua, "High-Accuracy Positioning Based on Pseudo-Ranges: Integrated Difference and Performance Analysis of the Loran System," Sensors, vol. 20, no. 16, p. 4436, 2020.

[38]. A. A. Kosti, Z. A. Anastassi, and T. E. Simos, "An Optimized Explicit Runge–Kutta Method with Increased Phase-Lag Order for the Numerical Solution of the Schrödinger Equation and Related Problems," Journal of Mathematical Chemistry, vol. 47, no. 1, pp. 315-330, 2009.

[39]. A. Alluhaybi, P. Psimoulis, and R. Remenyte-Prescott, "An Evaluation of Optimization Algorithms for the Optimal Selection of GNSS Satellite Subsets," Remote Sensing, vol. 16, no. 10, p. 1794, 2024.

[40]. S. Figiel, C. Specht, M. Moszyński, A. Stateczny, and M. Specht, "Testing of Software for the Planning of a Linear Object GNSS Measurement Campaign under Simulated Conditions," Energies, vol. 14, no. 23, p. 7896, 2021.

[41]. C. Chiarella, X.-Z. He, and C. Hommes, "A Dynamic Analysis of Moving Average Rules,"

In Press

Journal of Economic Dynamics and Control, vol. 30, no. 9-10, pp. 1729-1753, 2006.

[42]. C. C. Lin, L. S. Wang, F. R. Chang, and C. C. Chen, "Use of Residual DOP and Genetic Algorithm in Weighted-Least-Square GPS Positioning," Proceedings of the 2006 National Technical Meeting of the Institute of Navigation, pp. 508-514, 2006.

[43]. A. Tabatabaei, M. R. Mosavi, A. Khavari, and H. S. Shahhoseini, "Reliable Urban Canyon Navigation Solution in GPS and GLONASS Integrated Receiver using Improved Fuzzy Weighted Least-Square Method," Wireless Personal Communications, vol. 94, pp. 3181-3196, 2017.

Biographies

N. Dabaghi Daryan received her B.S., and M.S. degrees in Electronic Engineering from Iran University of Science and Technology (IUST), Tehran, Iran in 2021, and 2023, respectively. She is currently a Ph.D. student in the Department of Electrical Engineering at Iran University of Science and Technology (IUST). Her research interests include artificial intelligence, signal processing, and GNSS security and integrity.

M. R. Mosavi received his B.Sc., M.Sc., and Ph.D. degrees in Electronic Engineering from Iran University of Science and Technology (IUST), Tehran, Iran in 1997, 1998, and 2004, respectively. He is currently a faculty member (Full Professor) of the Department of Electrical Engineering of IUST. He is the author of more than 600 scientific publications in journals and international conferences in addition to 15 academic books. His research interests include circuits and systems design. He is also editor in-chief of "Iranian Journal of Marine Technology" and editorial board member of "Iranian Journal of Electrical and Electronic Engineering" and "GPS Solutions".

S. Mirzakuchaki received the B.Sc. degree in Electrical Engineering from the University of Mississippi in 1989 and the M.Sc. and Ph.D. degrees in Electrical Engineering from the University of Missouri-Columbia in 1991 and 1996, respectively. He has been a faculty member of the School of Electrical Engineering at Iran University of Science and Technology, Tehran, since 1996. His current research interests include digital systems and design of VLSI circuits.

S. Tohidi received her B.Sc. and M.Sc. degrees in Electronic Engineering from respectively Shahid Beheshti University and Malek Ashtar University of Technology, Tehran, Iran. She received Ph.D. degree in Electronic Engineering from Department of Electrical Engineering at Iran University of Science and Technology in 2023. Her research interests include signal processing, artificial intelligence, and GPS applications.

In Press

In Press